Applied Surface Science 255 (2009) 7115–7120

Contents lists available at ScienceDirect

Applied Surface Science

journal homepage: www.elsevier.com/locate/apsusc

Influence of $C_3H_8O_3$ in the electrolyte on characteristics and corrosion resistance of the microarc oxidation coatings formed on AZ91D magnesium alloy surface

Di Wu *, Xiangdong Liu, Kai Lu, Yaping Zhang, Huan Wang

School of Materials Science and Engineering, Inner Mongolia University of Technology, 49 Aimin Street, Hohhot 010051, PR China

ARTICLE INFO

Article history:
Received 11 January 2009
Received in revised form 25 February 2009
Accepted 25 February 2009
Available online 11 March 2009

PACS:
52.80−Mg
52.80−Wq
81.15−z
85.40−Sz

Keywords:
Magnesium alloy
Microarc oxidation
Coatings
Corrosion test

ABSTRACT

Ceramic coatings were fabricated on AZ91D Mg-alloy substrate by microarc oxidation in Na_2SiO_3–NaOH–Na_2EDTA electrolytes with and without $C_3H_8O_3$ addition. The effects of different concentrations of $C_3H_8O_3$ contained in the electrolyte on coatings thickness were investigated. The surface morphologies, RMS roughness, phase compositions and corrosion resistance property of the ceramic coatings were analyzed by scanning electron microscopy (SEM), atomic force microscopy (AFM), X-ray diffraction (XRD), and electrochemical corrosion test respectively. It is found that the addition of $C_3H_8O_3$ into silicate electrolyte leads to increase of the unit-area adsorptive capacity of the negative ions at anode–electrolyte interface and thus improves the compactness and corrosion resistance of the MAO coating. The coating thickness decreases gradually with the increase of concentrations of $C_3H_8O_3$ in the electrolyte. The oxide coating formed in base electrolyte containing 4 mL/L $C_3H_8O_3$ exhibits the best surface appearance, the lowest surface RMS roughness (174 nm) and highest corrosion resistance. In addition, both ceramic coatings treated in base electrolyte with and without $C_3H_8O_3$ are mainly composed of periclase MgO and forsterite Mg_2SiO_4 phase, but no diffraction peak of Mg phase is found in the patterns.

1. Introduction

Magnesium and its alloys have lots of outstanding performances such as low density, high specific strength and good electromagnetic shielding characteristics [1], which suggest that wide application of magnesium alloys is expected in the fields of automobile and aerospace industry. However, the poor corrosion resistance has hindered their widespread use in many applications, especially in acidic environment and in salt-water conditions [2]. Accordingly, it is of extraordinary importance to improve surface properties of magnesium alloys.

The microarc oxidation (MAO) is a new surface technology of producing ceramic coatings on valve metals, which is developed from anode oxidation [3–5]. Compared with conventional anodizing, the MAO treatment is achieved by using high alternative voltage and it implies electrochemical, plasma chemical and thermal chemical reactions taking place in the electrolyte [6,7]. With this method, ceramic coatings can be directly fabricated on the surface of magnesium alloys, the surface properties such as corrosion resistance, wear resistance, and microhardness can be improved considerably [8–11]. It has been found that the electrolyte compositions play a crucial role in the MAO process [12] and it is imperative to properly select the compositions of electrolyte.

In the present work, the $C_3H_8O_3$ was added into the silicate electrolyte so that a higher performance of ceramic coating with less pores and microcracks could be obtained by means of MAO treatment and its corrosion resistance property could be greatly improved. The influences of $C_3H_8O_3$ (added in Na_2SiO_3–NaOH–Na_2EDTA electrolyte) and its different concentrations on the thickness, surface morphology, the root-mean-square roughness and phase composition of the ceramic coatings were analyzed. In addition, the corrosion resistance of Mg alloy and oxidation coatings was also evaluated by means of electrochemical corrosion test.

2. Experimental details

The die-cast AZ91D magnesium alloy (mass fraction: Al 8.5–9.5%, Zn 0.5–0.9%, Mn 0.17–0.40%, Si ≤ 0.05%, Fe ≤ 0.004, balance Mg) was used as the substrate material in the present work. The dimension of the rectangular samples was 30 mm × 20 mm × 3 mm. Prior to

* Corresponding author. Tel.: +86 132 38415499; fax: +86 471 6575752.
E-mail address: wudiyhj0808@yahoo.cn (D. Wu).

0169-4332/$ – see front matter © 2009 Elsevier B.V. All rights reserved.
doi:10.1016/j.apsusc.2009.02.087

Table 1
Base electrolyte compositions and constant applied electrical parameters.

Base electrolyte composition		Constant applied electrical parameters	
		Forward/reverse voltages	Frequency
Na_2SiO_3 (analytically pure)	10 g/L	400/120 V	100 Hz
NaOH (analytically pure)	2 g/L		
Na_2EDTA (analytically pure)	2 g/L		

MAO processing, all the samples were polished with waterproof abrasive paper and degreased with acetone and followed by rinsing water.

The treatment device for MAO process consisted of a high power supply unit (WHD-30), a stainless steel container, a stirring and cooling system which maintained the electrolyte temperature below 35 °C through the circulation water during the process. In this work, the compositions of base electrolyte prepared with distilled water and constant applied electrical parameters were listed in Table 1, and the positive/negative current can be automatically adjusted by MAO power supply. The concentrations of $C_3H_8O_3$ in the electrolyte varied in the range of 0–6 mL/L. All the samples were treated in the electrolyte for 15 min.

The eddy current coating measurement gauge (HCC-25) was employed to measure thickness of ceramic coatings. The surface morphology and root-mean-square (RMS) roughness of the oxidation coatings were investigated by using a S-3400N scanning electron microscope (SEM) and a Benyuan CSPM-4000 atomic force microscopy (AFM) system. The software CSPM imager 4.60 was used for data processing and surface roughness analysis. The X-ray diffraction (XRD) analysis was performed by using an X-ray diffractometer (PW1700, Cu Kα radiation) to identify the different phases present in the coatings. The scans were acquired from 20° to 80° (in 2θ) at a scan rate of 3° min^{-1}.

The corrosion resistance of Mg alloy substrate and ceramic coatings were evaluated through SOLARTRON-1280B electrochemical corrosion test system, in which the samples with an exposed area of 4 cm^2 were immersed in 3.5 wt.% NaCl solution at the room temperature of 25 ± 2 °C. The reference electrode is saturated calomel electrode (SCE), and auxiliary electrode is Pt electrode. After 10 min of initial delay, scan was conducted with a constant rate of 10 mV/s from −2.5 V to reach 1.0 V potential.

3. Results and discussion

3.1. Thickness of ceramic coatings

The variation of thickness of ceramic coatings obtained through MAO treatment for 15 min in base electrolyte containing 0, 2, 3, 4, 5 and 6 mL/L $C_3H_8O_3$, respectively, are shown in Fig. 1. According to the plot, it is noticed that the thickness of ceramic coatings decreases gradually with the increase of concentration of $C_3H_8O_3$. The thickness of coating formed in base electrolytic solution without $C_3H_8O_3$ addition exhibits a high thickness value reaching about 111 μm. However, the addition of $C_3H_8O_3$ into the base electrolyte results in a decrease of the value of coatings thickness. As concentration of $C_3H_8O_3$ varies from 2 to 6 mL/L, the coating thickness decreases from 105 to 64 μm.

3.2. Surface morphology and root-mean-square (RMS) roughness of ceramic coatings

Fig. 2 illustrates the surface morphology of ceramic coatings fabricated on magnesium alloys by MAO treated for 15 min in the base electrolyte without and with $C_3H_8O_3$ addition. According to the SEM images (at low magnification), it is found that numerous

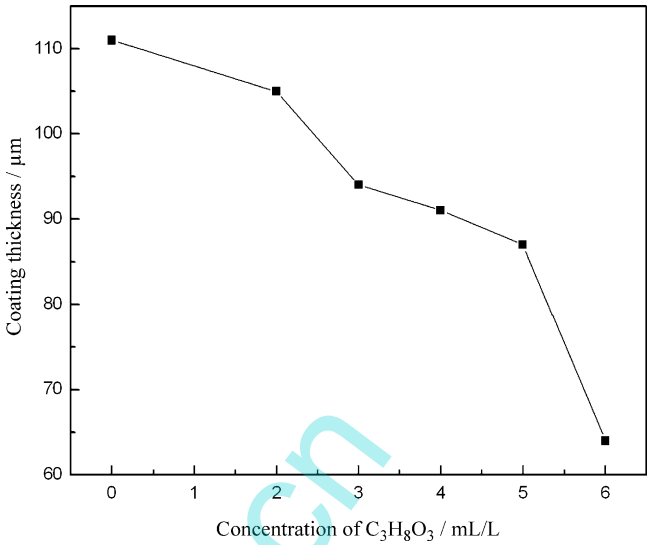

Fig. 1. Variation of thickness of ceramic coatings obtained through MAO for 15 min in base electrolyte with different concentrations of $C_3H_8O_3$.

micropores appearing as circular spots and some microcracks, micropits are present on top of the coatings surface, regardless of the coatings made from in different electrolyte. In Fig. 2a, the pores in the coating are not homogeneous either in dimension or in distribution. Nevertheless, the addition of $C_3H_8O_3$ leads to an obvious change in the surface morphology of ceramic coatings. In other words, the ceramic coatings obtained in base electrolyte with $C_3H_8O_3$ of which surface morphologies are shown in Fig. 2b–d have much smaller pores and less microcracks than that obtained in the base electrolytic solution. In particular, as for the coatings prepared in the base electrolyte with different concentrations of $C_3H_8O_3$, the coating formed in the base electrolyte containing 4 mL/L $C_3H_8O_3$ exhibits the micropores with the smallest size and the least microcracks in this work. At the same time, this coating has uniform-size and uniform-distribution micropores.

At a higher magnification (Fig. 2e and f), it is found that the coating prepared from $C_3H_8O_3$-free electrolyte has a large pore diameter about 8.5 μm (average size) while that prepared from electrolyte with 4 mL/L $C_3H_8O_3$ addition has a small pore diameter about 2.63 μm. In addition, according to the Fig. 2e, it is also obviously found that some smaller pores are unevenly distributed inside of the larger solidified micropits. It has been reported that the morphology characteristic of the MAO coating is consistent with the sparking discharge phenomena of the substrate [13]. Thus, the reasons for the phenomenon could be probably explained as follows: on the one hand, in the base electrolyte, the individual larger discharge sparking due to high discharge energy and instability of the microarc oxidation process appears on the coating, which leads to the formation of the larger micropits. On the other hand, the discharge breakdown occurs repeatedly on such micropit where the coating thickness is thin enough so that it becomes the relatively weak position for discharge breakdown during the MAO treatment. Consequently, there are lots of defects on the coating formed in base electrolyte without $C_3H_8O_3$. However, the addition of $C_3H_8O_3$ into the base electrolyte give rise to maintaining the stability of the microarc oxidation process and the numerous intensive discharge sparks with small size appear on the coating during the MAO treatment, which results in the pores homogeneous in smaller size and distribution over the ceramic coatings, as illustrated in Fig. 2f.

Glycerol is a polar liquid with many free and strong polar hydroxyl groups, a high dielectric constant and surface activity at the solid–liquid interface, which gives rise to specific adsorption at

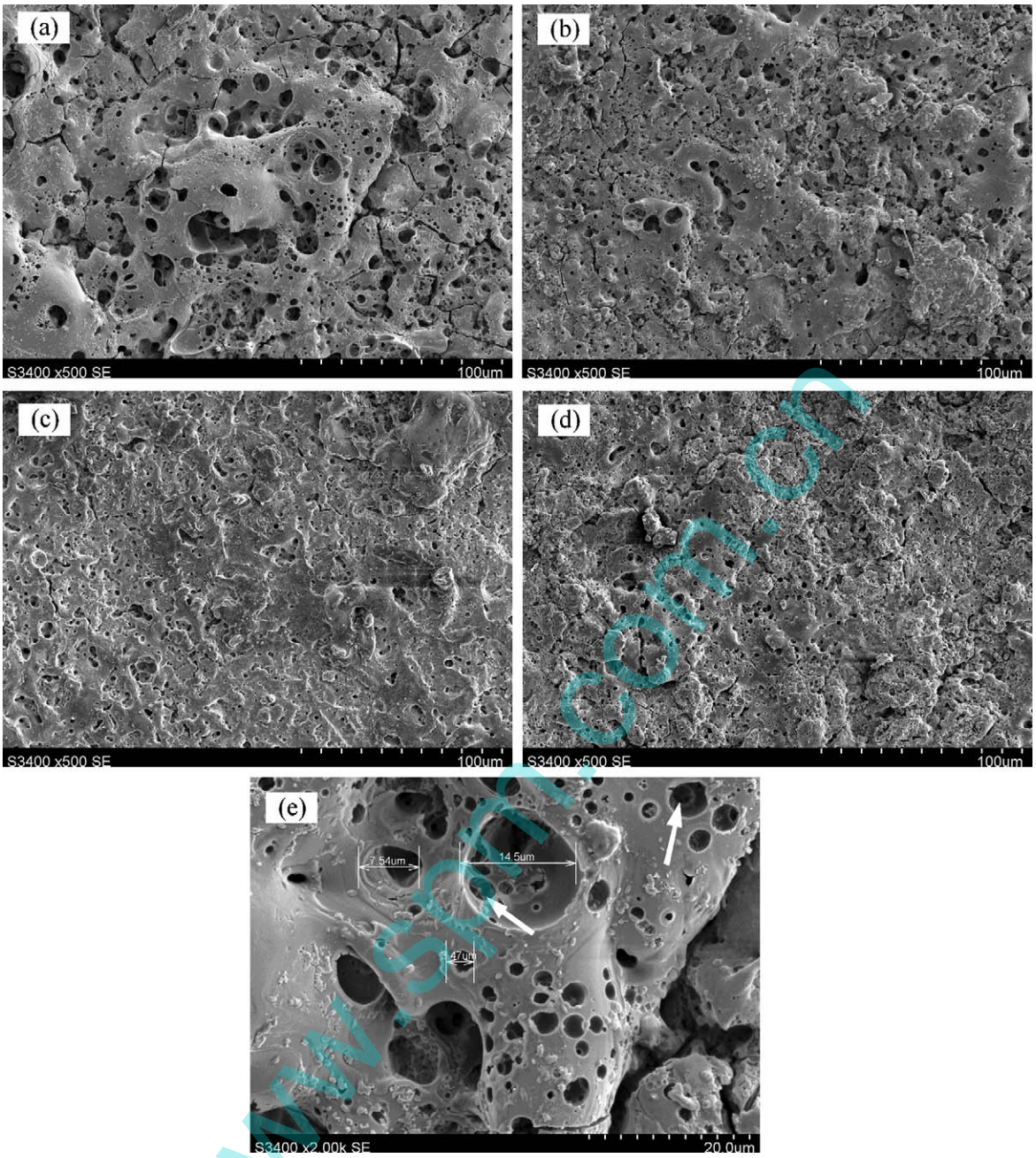

Fig. 2. SEM images of ceramic coatings fabricated on the surface of magnesium alloys treated for 15 min in base electrolyte containing different concentrations of $C_3H_8O_3$. (a) Without $C_3H_8O_3$; (b) with 2 mL/L $C_3H_8O_3$; (c) with 4 mL/L $C_3H_8O_3$; (d) with 6 mL/L $C_3H_8O_3$; (e) a high magnification view of (a); (f) a high magnification view of (c).

the interface between anode and electrolyte in alkali solutions [14]. The model for adsorbed layer of C3H8O3 molecules at interface is shown in Fig. 3b. It possibly substitutes for the H2O molecular film formed at the anode–electrolyte interface in the base electrolyte, to some extent, which leads to decrease of the solid–liquid interfacial tension. Accordingly, the unit-area adsorptive capacity of the negative ions close to anode–electrolyte interface has been increased in number as a result of the spreadability of the electrolyte at the interface. In addition, as a matter of fact, the anions ionized from Na_2SiO_3 solution predominantly exist in the form of $[SiO(OH)_3]^-$ and $[Si(OH)_2]_2^-$ anions rather than SiO_3^{2-} in the electrolyte, and the poly-silicic acid (PSA) particles with negative electricity are formed finally through hydrolytic and polymeritic reactions concerning the above anions[15,16], the structure as shown in Fig. 4. Both the PSA particle and $C_3H_8O_3$ molecule have the same structure with –OH groups. That is to say, the $C_3H_8O_3$ molecules tend to be adsorbed around the PSA particle due to the fact that they have the similar polarity and affinity each other. So, it is possible to conclude that the interparticle repulsive force decreases with adsorption of more $C_3H_8O_3$ molecules around the particle giving rise to decrease of surface tensions of these negative particles which has been arranged much more densely at the anode–electrolyte interface under the action of electric field force. These lead to formation of the dense and uniform discharge centers on the surface of passivated coating during the MAO process, and then the passivated coating has been turned into dense, uniform ceramic coating by the action of electric breakdown, particles melting and sintering. So, the ceramic coating obtained in electrolyte with proper content of $C_3H_8O_3$ have smoother surface, less pores and

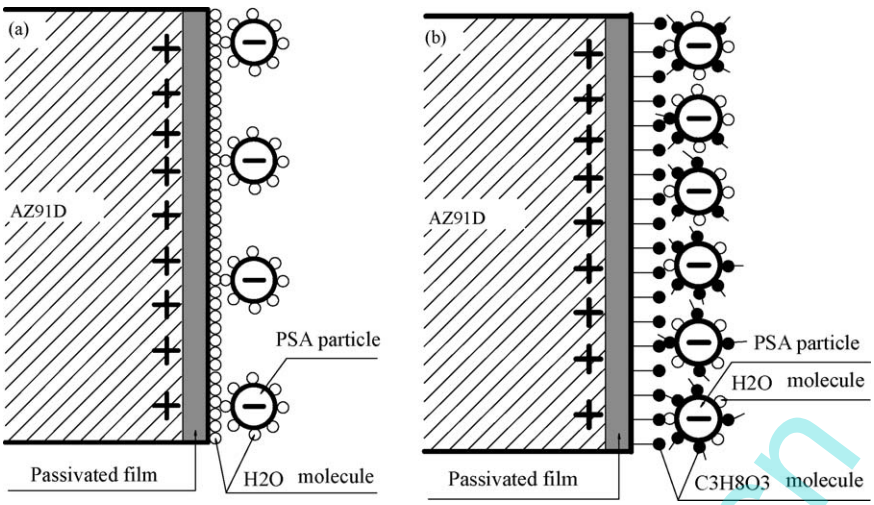

Fig. 3. Schematic illustration of the particles distribution at anode/electrolyte interface in two different electrolyte at the primary stages of the MAO treatment. (a) In the base electrolyte; (b) in base electrolyte containing $C_3H_8O_3$.

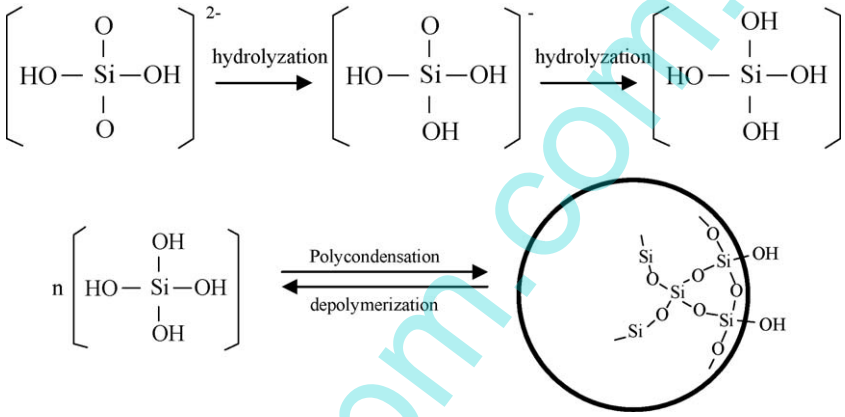

Fig. 4. The structure of poly-silicic acid particle and its formation process.

microcracks than that obtained in the base electrolytic solution. Thus, the compacter structure of the coating decreases the passages for the eroding anions entering into the coating and thus provides a superior corrosion resistance.

The average values of the root mean square (RMS) roughness of ceramic coatings formed in base electrolyte containing different concentrations of $C_3H_8O_3$ were analyzed using the AFM software, as presented in Fig. 5. The AFM scan was performed in at least five different regions for each coated samples surface, and the scattering region is 12.807 μm × 12.807 μm. In accordance with the surface morphology, the surface roughness of ceramic coatings decreases first and then increases somewhat with increasing the concentration of $C_3H_8O_3$ addition into the base electrolyte. The coating formed in $C_3H_8O_3$-free electrolyte displays the highest average value of RMS roughness reaching 424 nm while that obtained in base electrolyte containing 4 mL/L $C_3H_8O_3$ exhibits the lowest average value of RMS roughness reaching 174 nm.

The ceramic coating obtained in the base electrolyte displays the high surface roughness partly due to the different deposition rate of ceramic coating in every direction during electrolytic deposition process. Nevertheless, the $C_3H_8O_3$ molecules could be adsorbed preferentially by those crystal faces with high activity and fast formation rate, where the resistance force of electrochemical reaction increases after the addition of $C_3H_8O_3$ into the base electrolyte. So, in that case, it is possible to obtain uniform deposition rate in every crystal face and promote to form the ceramic coating with dense structure and better smoothness. However, when the excessive $C_3H_8O_3$ added in the base electrolyte, an increasing number of $C_3H_8O_3$ molecules are adsorbed around the PSA particles by which the electronegativity of PSA particles has been sharply decreased. This accelerates the gelatinization of

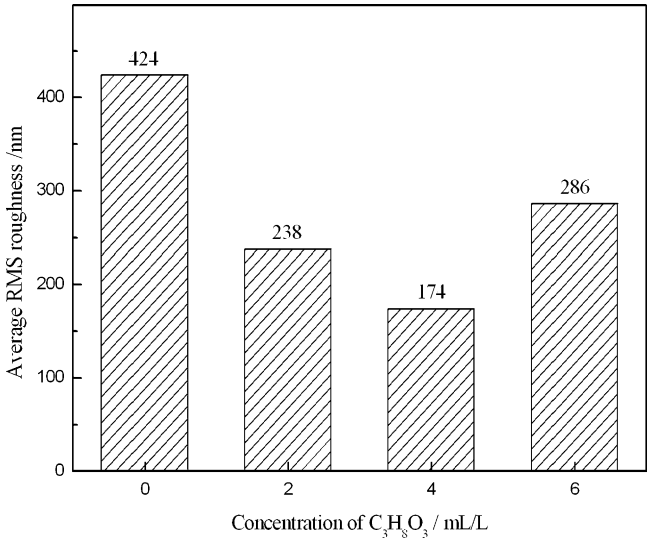

Fig. 5. The average RMS roughness of ceramic coatings formed in base electrolyte with different concentrations of $C_3H_8O_3$.

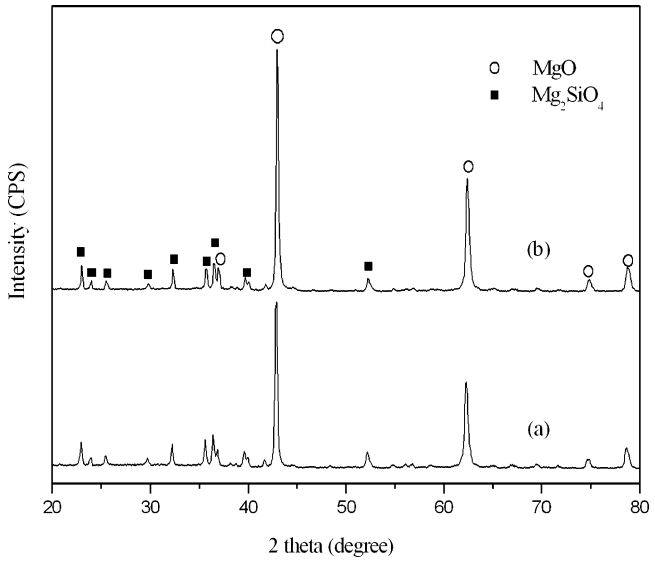

Fig. 6. The XRD patterns of ceramic coating formed in base electrolyte without and with $C_3H_8O_3$ addition by MAO (a) without $C_3H_8O_3$ addition; (b) with C3H8O3 addition of 4 mL/L.

the PSA particles and thus weakens the ability of substance transmission to the anode surface during MAO process, which leads to sharp decrease of the coating formation rate and non-uniform deposition on the coating surface. Therefore, the roughness of treated specimen in electrolyte with a 6 mL/L is even larger than that of treated specimen with a 4 mL/L.

3.3. Phase composition

Fig. 6 illustrates the XRD patterns of MAO ceramic coatings processed for 15 min in base electrolyte without and with 4 mL/L $C_3H_8O_3$ addition. According to the pattern, it can be seen that both ceramic coatings treated in two different electrolytes are mainly composed of periclase MgO and forsterite Mg_2SiO_4 phase, and no peaks associated with $C_3H_8O_3$ are found. Compared with Fig. 6a, the intensity of the MgO phase increase in Fig. 6b. It is well known that the relative content of detected phases in the coating is judged based on the intensities of the diffraction peaks corresponding to the phases in XRD patterns [17]. Accordingly, as for the oxide coating formed in electrolyte with $C_3H_8O_3$ addition, the relative content of the MgO increases in the coating, which suggests that the oxidation of Mg substrate has been promoted on the sample surface. It is attributed to a relative increase of resistance force of electrochemical reaction at anode–electrolyte interface with the addition of $C_3H_8O_3$, and at the same time, more Mg^{2+} and O^{2-} has been accumulated until the dielectric has been broken down during the MAO process. Unexpectedly, there are not peaks of Mg phase in the XRD pattern. In view of the result, it can be inferred that the X-ray appears to be not penetrate through to the magnesium substrate, thus, indicating that the both coatings obtained in base electrolyte with and without $C_3H_8O_3$ addition have a rather compact structure.

3.4. Corrosion resistance property

The corrosion behavior of the coatings is investigated by the electrochemical potentiodynamic polarization in 3.5 wt.% NaCl solution. Fig. 7 demonstrates the potentiodynamic polarization curves of AZ91D substrate and coated samples formed in base electrolyte with and without $C_3H_8O_3$ addition. The corrosion potential (E_{corr}) and the corrosion current density (i_{corr}) derived from the potentiodynamic polarization curves are shown in Table 2.

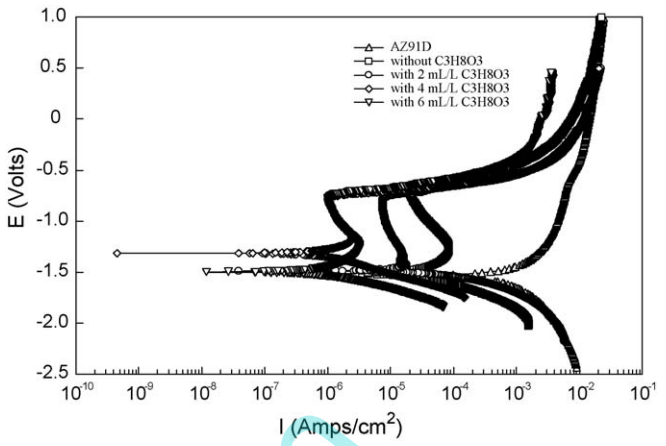

Fig. 7. Potentiodynamic polarization curves of the coatings formed in different conditions and AZ91D alloy substrate in 3.5 wt.% NaCl solution.

Table 2
The results of the potentiodynamic corrosion tests in 3.5 wt.% NaCl solution.

Samples	E_{corr} (V)	i_{corr} (A/cm^2)
AZ91D	−1.535	8.89×10^{-4}
0 mL/L $C_3H_8O_3$	−1.512	6.16×10^{-5}
2 mL/L $C_3H_8O_3$	−1.483	5.07×10^{-5}
4 mL/L $C_3H_8O_3$	−1.313	5.18×10^{-7}
6 mL/L $C_3H_8O_3$	−1.486	5.69×10^{-7}

Generally speaking, the high corrosion potential and low corrosion current density of the coating suggests that it exhibits a low corrosion rate and a good corrosion resistance [18,19]. The data listed in Table 2 clearly show that all of oxide films of the samples treated by MAO in base electrolyte with and without $C_3H_8O_3$ addition, without exception, exhibits more positive E_{corr} and lower i_{corr} than that of AZ91D substrate, which indicates that the anti-corrosion property of the magnesium alloy surface has been improved considerably after MAO treatment. Moreover, compared with the coating treated in base electrolyte, the ceramic coatings formed in electrolytic solution containing $C_3H_8O_3$ have higher corrosion potential and lower current density, thus it can be concluded that the coatings prepared using base electrolyte with addition of $C_3H_8O_3$ have lower corrosion rate and better corrosion resistance than that of formed in electrolyte without $C_3H_8O_3$. In addition, as for the coatings obtained in electrolyte with $C_3H_8O_3$, with the increase of concentration of $C_3H_8O_3$ in the electrolyte, the corrosion potential increases and the corrosion current density decreases except for the coating formed in 6 mL/L $C_3H_8O_3$. The coating formed in base electrolyte with 4 mL/L $C_3H_8O_3$ exhibits the most positive corrosion potential (−1.313 V) and the lowest corrosion current density (5.18×10^{-7} A/cm^2). In contrast to the AZ91D substrate, the E_{corr} increases by 222 mV while the i_{corr} decreases by nearly three orders of magnitude. That is to say, the lowest corrosion rate is displayed by the coating formed in the electrolyte containing 4 mL/L $C_3H_8O_3$. It can be attributed to the fact that the smaller micropores and less microcracks, as well as relatively uniform structure on this coating, decreases the passages for the eroding Cl^- anions entering into the coating and thus provides a superior corrosion resistance.

4. Conclusions

The following conclusions can be drawn from this work, relating to MAO ceramic coatings obtained on AZ91D magnesium alloy in the base electrolyte with and without $C_3H_8O_3$ addition.

1. The thickness of ceramic coatings decreases gradually from 111 to 64 μm with the increasing concentration of C3H8O3 from 0 to 6 mL/L.
2. Numerous micropores and some microcracks, micropits are present on top of the coatings surface of all coated samples. However, the addition of $C_3H_8O_3$ into base electrolyte results in decrease of the number and size of micropores as well as the microcracks. Moreover, the surface RMS roughness of ceramic coatings decreases first and then increases somewhat with increasing the concentrations of $C_3H_8O_3$ addition into base electrolyte according to the AFM technology. In particular, The ceramic coating formed in base electrolyte containing 4 mL/L C3H8O3 exhibits the best surface appearance and lowest surface RMS roughness (174 nm) as compared with that of any other coated sample in this work.
3. It is found from XRD analysis that both MAO ceramic coatings treated in base electrolyte with and without $C_3H_8O_3$ addition are mainly composed of periclase MgO and forsterite Mg_2SiO_4 phase, but no diffraction peak of Mg phase is found in the patterns. In addition, the relative content of the MgO increases whereas the Mg_2SiO_4 phase decreases somewhat in the coating as the addition of $C_3H_8O_3$ into base electrolyte.
4. The lowest corrosion rate is displayed by the coating formed in the electrolyte containing 4 mL/L $C_3H_8O_3$ which exhibits the most positive corrosion potential (−1.313 V) and the lowest corrosion current density (5.18×10^{-7} A/cm^2) by means of electrochemical corrosion test in 3.5 wt.% NaCl solution.

Acknowledgements

This work was supported by the Key Scientific and Technological Project Foundation of Inner Mongolia Autonomous Region, P.R. China, under the contract no. 20040202.

References

[1] J.E. Gray, B. Luan, J. Alloys Compd. 336 (2002) 88.
[2] G.L. Song, A. Atrens, Adv. Eng. Mater. 5 (2003) 837.
[3] A.L. Yerokhin, X. Nie, A. Leyland, A. Matthews, S.J. Dowey, Surf. Coat. Technol. 122 (1999) 73.
[4] J. Liang, L.T. Hu, J.C. Hao, Appl. Surf. Sci. 253 (2007) 4490.
[5] M.F. Hsieh, L.H. Perng, T.S. Chin, Mater. Chem. Phys. 74 (2002) 245.
[6] F. Mécuson, T. Czerwiec, T. Belmonte, L. Dujardin, A. Viola, G. Henrion, Surf. Coat. Technol. 200 (2005) 804.
[7] S.G. Xin, L.X. Song, R.G. Zhao, X.F. Hu, Thin Solid Films 515 (2006) 326.
[8] X.P. Zhang, Z.P. Zhao, F.M. Wu, Y.L. Wang, J. Wu, J. Mater. Sci. 42 (2007) 8523.
[9] A.L. Yerokhin, A. Shatrov, V. Samsonov, P. Shashkov, A. Leyland, A. Matthews, Surf. Coat. Technol. 182 (2004) 78.
[10] H.F. Guo, M.Z. An, Thin Solid Films 500 (2006) 186.
[11] W.B. Xue, Z.W. Deng, R.Y. Chen, T.H. Zhang, Thin Solid Films 372 (2000) 114.
[12] P.I. Butyagin, Ye.V. Khokhryakov, A.I. Mamaev, Mater. Lett. 57 (2003) 1748.
[13] Y.Q. Wang, K. Wu, M.Y. Zheng, Surf. Coat. Technol 201 (2006) 353.
[14] L.M. Feng, Y. Wang, Sun Fs H., Electroplating Technology and Equipments, Chemical Industry Press, Beijing, 2005, in Chinese.
[15] Z. Shen, G.T. Wang, Colloid and Surface Chemistry, Chemical Industry Press, Beijing, 1997, in Chinese.
[16] X.F. Yang, P. Roonasi, H. Allan, J. Colloid Interface Sci. 328 (2008) 41.
[17] A.L. Yerokhin, L.O. Snizhko, N.L. Gurevina, A. Leyland, A. Matthrews, J. Phys. D: Appl. Phys. 36 (2003) 2110.
[18] J. Liang, B.G. Guo, J. Tian, H.W. Liu, J.F. Zhou, W.M. Liu, T Xu, Surf. Coat. Technol. 199 (2005) 121.
[19] Y. Zhang, C. Yan, F. Wang, H. Lou, C. Cao, Surf. Coat. Technol. 161 (2002) 36.